The neuroreceptors and transporters underlying spontaneous brain activity

Johan Nakuci[1]* and Kanika Bansal[1,2]

[1]U.S. Army DEVCOM Army Research Laboratory, Aberdeen Proving Ground, Aberdeen, MD, 21005, USA
[2]Computer Science and Electrical Engineering, University of Maryland Baltimore County, Baltimore, MD, 21250, USA
*Corresponding author Email: jnakuci@gmail.com

Competing Interest Statement: The authors declare no competing interests.

Keywords: resting-state fMRl, neuroreceptors, excitation-inhibition balance, neuropsychiatric illness, LSD, Modafinil, structural and geometric eigenmodes

Acknowledgements: We would like to thank Javier Garcia, Jessie J Polanco and Italo'Ivo Lima Dias Pinto for their thoughtful comments. This research was supported by the U.S. Army DEVCOM Army Research Laboratory through army educational outreach program (W911SR-15-2-0001). The views and conclusions contained in this document are those of the authors and should not be interpreted as representing the official policies, either expressed or implied, of the U.S. Army DEVCOM Army Research Laboratory or the U.S. Government. The U.S. Government is authorized to reproduce and distribute reprints for Government purposes notwithstanding any copyright notation herein.

Author Contributions:
Conceptualization: JN
Methodology: JN
Data Curation: JN
Visualization: JN
Funding acquisition: JN, KB
Writing – original draft: JN, KB
Writing – review & editing: JN, KB

Abstract

Identifying the neuromodulators driving brain activity is critical for understanding communication, cognition, and neuropathology. Neuromodulators act through neuroreceptors and transporters and crucially, operate in a coordinated manner. However, *in vivo* methods in humans that can identify the neuromodulators driving brain activity remain limited. Here, we address this limitation using a neuroreceptor-based framework, enabling the identification of neuroreceptors and transporters underlying spontaneous brain activity. The framework utilizes cortical density maps of 19 neuroreceptors and transporters derived from Positron Emission Tomography (PET). Across four datasets ($N_{total} = 314$), our framework reconstructs spontaneous brain activity and functional connectivity (FC) from BOLD signals measured by functional MRI (fMRI), achieving an average accuracy of $R_{BOLD} = 0.58 \pm 0.05$ and $R_{FC} = 0.62 \pm 0.02$. Notably, our analysis reveals that the excitation-inhibition balance is maintained by two distinct modules of neuroreceptors and transporters exhibiting regional density differences across the cortex. The framework's validity is supported by its ability to recover neuroreceptors and transporters — 5-HT1a, 5-HT1b, 5-HT2a, and D2 — known to bind lysergic acid diethylamide (LSD), and D2, 5-HT1a, 5-HT2a, and NET mediating the effects of Modafinil. Furthermore, the framework identified mechanistic links between neuroreceptors, transporters, and altered brain activity in schizophrenia, bipolar disorder, and ADHD. Finally, neuroreceptor-based reconstruction outperformed models based on structural connectivity and cortical folding geometry. Together, these findings underscore the potential of this neuroreceptor-based framework to advance our understanding of neuromodulatory mechanisms across diverse brain states and conditions.

Introduction

At any given moment, across the brain, a diverse array of neuromodulators binds to and unbinds from neurons driving activity. The complexity of this process becomes evident when considering that the human brain utilizes over 100 neuromodulators across approximately 10^{11} neurons, each forming an average of 1,000 unique connections[1]. Neuromodulators act through corresponding neuroreceptors and transporters and crucially no individual neuromodulator works alone, instead their actions are coordinated[2]. This intricate interplay poses a significant challenge in identifying which specific neuromodulators drive brain activity at any moment.

Neuromodulators can induce either excitation or inhibition, enabling the brain's vast computational capabilities[3]. Moreover, the balance between excitatory and inhibitory inputs dynamically changes over time, reflecting different brain states[4]. These fluctuations have been linked to aging[5], psychosis[6] and can impact cognitive processes and behaviors across diverse domains, including social interactions[7], economic decisions[8], and even perception[9].

In vivo, neuromodulators can be determined using fluorescent probes[10,11], microdialysis[12], or electrochemistry[13]. However, these methods provide limited insights as they typically measure only a few neuromodulators at a time or are restricted to a subset of brain regions[14]. Expanding the available tools would open new avenues for understanding how neuromodulators are coordinated across the cortex to shape cognition and behavior in healthy and pathological brain states. Moreover, the invasive nature of *in vivo* methods limits their application in humans, underscoring the need for a non-invasive approach to determine the neuromodulators driving brain activity[15].

The concentration of neuroreceptors is an important factor in mediating the effects of neuromodulators on brain activity, as these serve as the primary sites for excitatory synaptic inputs[16], dynamically changing in response to neural activity, stimuli and conditions[17], and can shape long-term memory[18]. The concentration of neuroreceptors across the brain can be non-invasively estimated using PET tracer imaging[19,20]. Moreover, recent work has shown that neuroreceptors shape brain-wide communication estimated from the BOLD signal[21–23]. This association suggests that combining neuroreceptor density maps estimated from PET imaging

with the BOLD signal could be a non-invasive method to uncover the neuromodulators that drive brain activity across the human cortex and unravel the complex mechanisms that underlie cognition and behavior.

Here we use a linear modeling framework that reconstructs the BOLD signal through a weighted summation of PET-derived neuroreceptor and transporter density maps. The modeling framework reveals an underlying network architecture that captures dynamic interactions between neuroreceptors, transporters and spontaneous brain activity. Specifically, the BOLD signal emerges from a coordinated interplay among two modules of neuroreceptors and transporters. We validate these findings in two additional datasets and show that the neuroreceptor-based framework recovers neuroreceptors and transporters linked to the binding profiles of LSD and in mediating the effects of Modafinil. Extending this framework, we identify a mechanistic link between neuroreceptors, transporters, and altered brain activity across several neuropsychiatric disorders. Finally, we demonstrate that the neuroreceptor-based framework outperforms models based on anatomical factors in reconstructing brain activity, highlighting its predictive power.

Results

<u>Reconstructing the BOLD signal and functional connectivity from neuroreceptor and transporter maps</u>

To determine if neuroreceptor and transporter density maps could non-invasively reveal the neuromodulators that drive spontaneous brain activity, we assessed whether a linear modeling framework could reconstruct the temporal dynamics of the BOLD signal. We utilize the most comprehensive neuroreceptors and transporters cortical density maps to date as detailed in Hansen *et. al*[24]. In brief, PET tracer imaging from a combined 1,238 healthy individuals was used to map the densities of 19 neuroreceptors and transporters from 9 neuromodulator systems: dopamine (D1, D2, DAT), norepinephrine (NET), serotonin (5-HT1A, 5-HT1B, 5-HT2A, 5-HT4, 5-HT6, 5-HTT), acetylcholine (α4β2, M1, VAChT), glutamate (mGluR5, NMDA), γ-aminobutyric acid (GABAa), histamine (H3), cannabinoid (CB1), and opioid neuroreceptor (MOR; **Fig. S1**). For each neuroreceptor and transporter, we estimated the average density within 200 brain regions based on the local-global parcellation of the human cerebral cortex estimated

from resting-state fMRI by Schaefer *et. al.*, because voxel-wise estimates can be unstable and noisy[25].

Spontaneous brain activity was estimated from 15 minutes of resting-state fMRI (N = 48) part of the Human Connectome Project (HCP)[26]. The extensive scanning duration of the HCP dataset allowed for an estimation of the relationship between neuroreceptors, transporters, and brain activity across a broader range of neural states. The voxelwise BOLD signal from each participant was averaged across the same brain regions defined by the Schaefer atlas, resulting in 200 x 1,200 data points per participant and 200 x 57,600 data points across all participants. Independently, each of the 57,600 time points of the BOLD signal were reconstructed from a weighted linear summation of the 19 neuroreceptor and transporter density maps (**Fig. 1A**). To quantify the effectiveness of the neuroreceptor-based framework, Pearson's correlation was used to estimate the accuracy between the reconstructed and the empirical brain maps for each of the 57,600 time points.

Focusing on a representative participant to demonstrate the effectiveness of the neuroreceptor-based framework, the BOLD signal at each moment in time was reconstructed with an average accuracy of $R_{BOLD_subj24} = 0.53 \pm 0.08$ (mean ± std; **Fig. 1B**). Comparable accuracy was observed across all participants ($R_{BOLD} = 0.51 \pm 0.08$; **Fig. 1C**). The observed reconstruction accuracy was significantly greater than that obtained from null models based on spatially permuted neuroreceptor and transporter maps ($P_{spatial} < 0.001$) and from a permutation that preserved the spatial auto-correlation, spin test ($P_{spin} < 0.001$; **Fig. 1D**)[27].

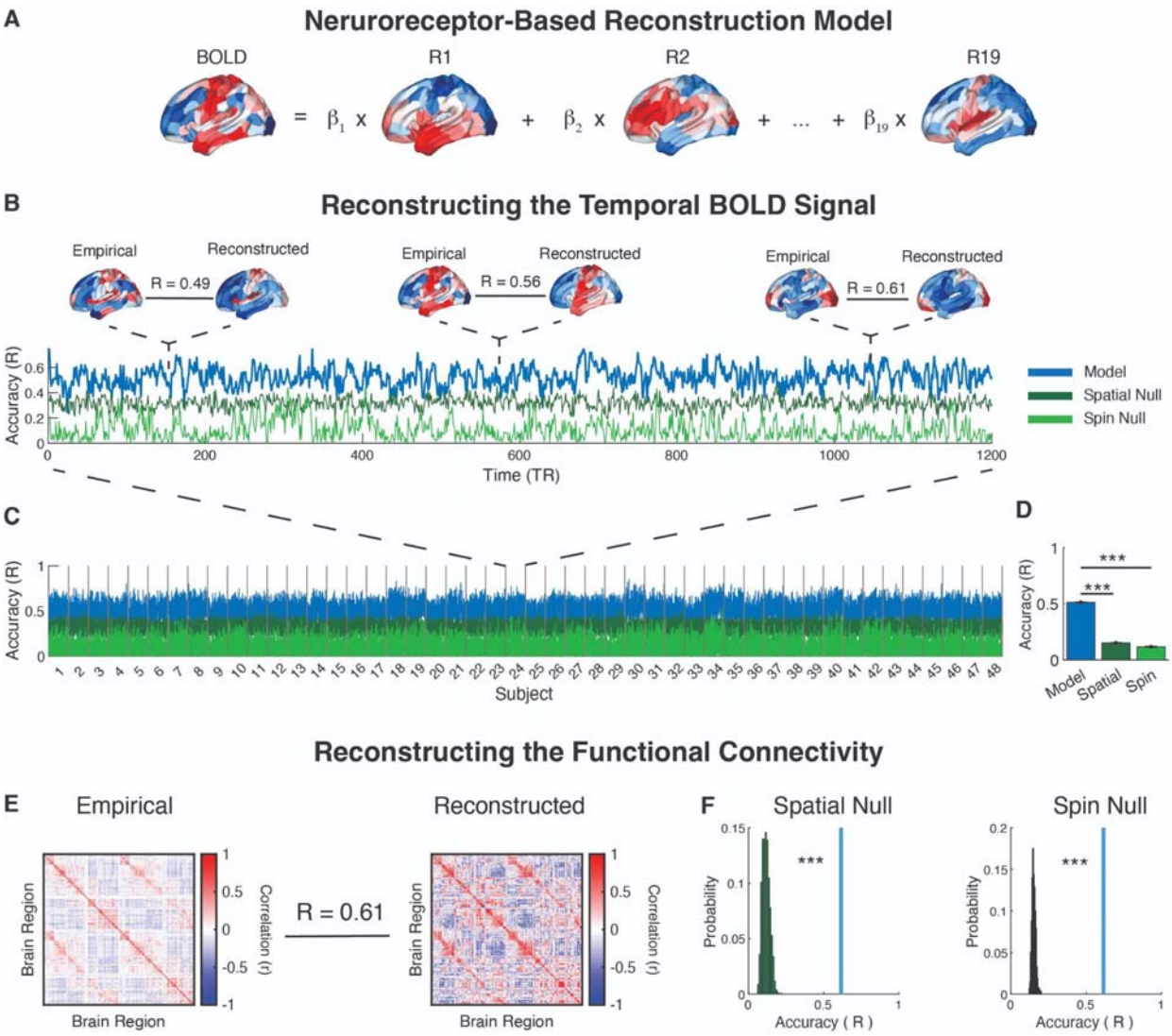

Figure 1. Neuroreceptor-based framework can reconstruct the BOLD signal and functional connectivity. (A) Neuroreceptor-based framework schematic. The BOLD signal was reconstructed from a linear summation of 19 neuroreceptors and transporters (R_1 to R_{19}) each weighted by corresponding coefficients (β_1 to β_{19}). For visualization purposes we have omitted the constant term in the model. (B) Reconstruction accuracy of the BOLD signal. Accuracy of neuroreceptor-based framework in reconstructing the BOLD signal over time in a representative participant. Pearson's correlation was used to estimate the accuracy between the reconstructed and the empirical brain maps. Brain plots depict the empirical, reconstructed brain and the accuracy between brain maps for representative time points. Line plots depict the accuracy over time. Blue line reflects the observed accuracy of the neuroreceptor-based model. Dark and light green lines reflect the accuracy from spatially permuted (spatial null) and spin-permutation (spin null) null models. (C) Group level reconstruction accuracy for each of the 1,200 time points per participant. (D) Neuroreceptor-based reconstruction is significantly greater than spatial and spin null models. Bar plots show the average accuracy at the group-level and for the spatial and spin null models. Error bars show mean ± sem. (E) Reconstructing functional connectivity. Accuracy

of reconstructing the group-level functional connectivity. The BOLD signal was concatenated across participants and Pearson's correlation was used to estimate the empirical functional connectivity (*left*). The reconstructed BOLD signal was concatenated across participants and Pearson's correlation was used to estimate the functional connectivity (*right*). (F) Comparison with spatial and spin null models. Blue line depicts the accuracy value from panel D. For both null models, the functional connectivity was estimated from the reconstructed BOLD signal by first concatenating the signal across participants followed by Pearson's correlation. ***P < 0.001.

Further, given that spontaneous brain activity exhibits coordination, or functional connectivity, among brain regions, we determined whether the reconstructed BOLD signal preserved this inherent property. Moreover, reconstructing the BOLD signal from neuroreceptor and transporter density does not inherently guarantee that the reconstruction will preserve FC at a comparable level. Thus, the ability to accurately reconstruct the inherent FC would validate the reliability of the modeling results. Conversely, if the reconstruction were dominated by random noise, the inherent FC would not be accurately reproduced.

To assess whether the reconstructed BOLD signal preserved inherent functional connectivity, we concatenated the empirical and reconstructed BOLD signals across participants and used Pearson's correlation to estimate the empirical and reconstructed functional connectivity networks, respectively. The reconstructed functional connectivity demonstrated comparable accuracy to that observed in the temporal BOLD signal ($R_{FC} = 0.61$; **Fig. 1E**) and was significantly greater than both null models ($P_{spatial} < 0.001$; $P_{spin} < 0.001$; **Fig. 1F**). Together, these findings highlight that a neuroreceptor-based framework can accurately reconstruct spontaneous brain activity and its inherent functional connectivity.

<u>Two distinct modules of neuroreceptors and transporters underlie dynamic brain activity</u>

No neuroreceptor or transporter acts in isolation; their actions are inherently coordinated[2]. For instance, the interplay among neuroreceptors and transporters associated with acetylcholine, dopamine, noradrenaline, and serotonin plays a crucial role in modulating brain activity associated with attention[28] and working memory maintenance[29]. However, most studies are limited to investigating only a few neuroreceptors and transporters at a time and therefore a comprehensive view is crucially lacking. We then investigated if the neuroreceptor-based

framework could provide a holistic view of neuroreceptors and transporters working together to drive brain activity. Specifically, we investigated whether model-derived drive values (i.e., β-values), which quantify the contributions of individual neuroreceptors and transporters to the BOLD signal, could identify the specific set of neuroreceptors and transporters working in congruence to drive fluctuations in brain activity.

As shown in Figure 2A, these drive values (i.e. β-values) exhibit marked fluctuations over time within a participant. To explore the relationship between drive values and dynamic brain activity, we focused on three representative neuroreceptors—GABAa, M1 muscarinic, and H3 histamine—that bind different neuromodulators (**Fig. 2B**). From Figure 2B, two observations are apparent. First, GABAa, M1 and H3 demonstrated periods of both positive and negative associations with the BOLD signal, indicating dynamic relationship with brain activity. Second, GABAa and M1 exhibited strong temporal coordination in drive values, while H3 showed an inverse relationship with both. These observations suggest that fluctuations in brain activity reflect coordination among multiple and distinct neuroreceptors and transporters. Understanding how neuromodulatory systems influence the emergent patterns of brain activity and cognitive processes requires quantifying the extent of temporal coordination among neuroreceptors and transporters.

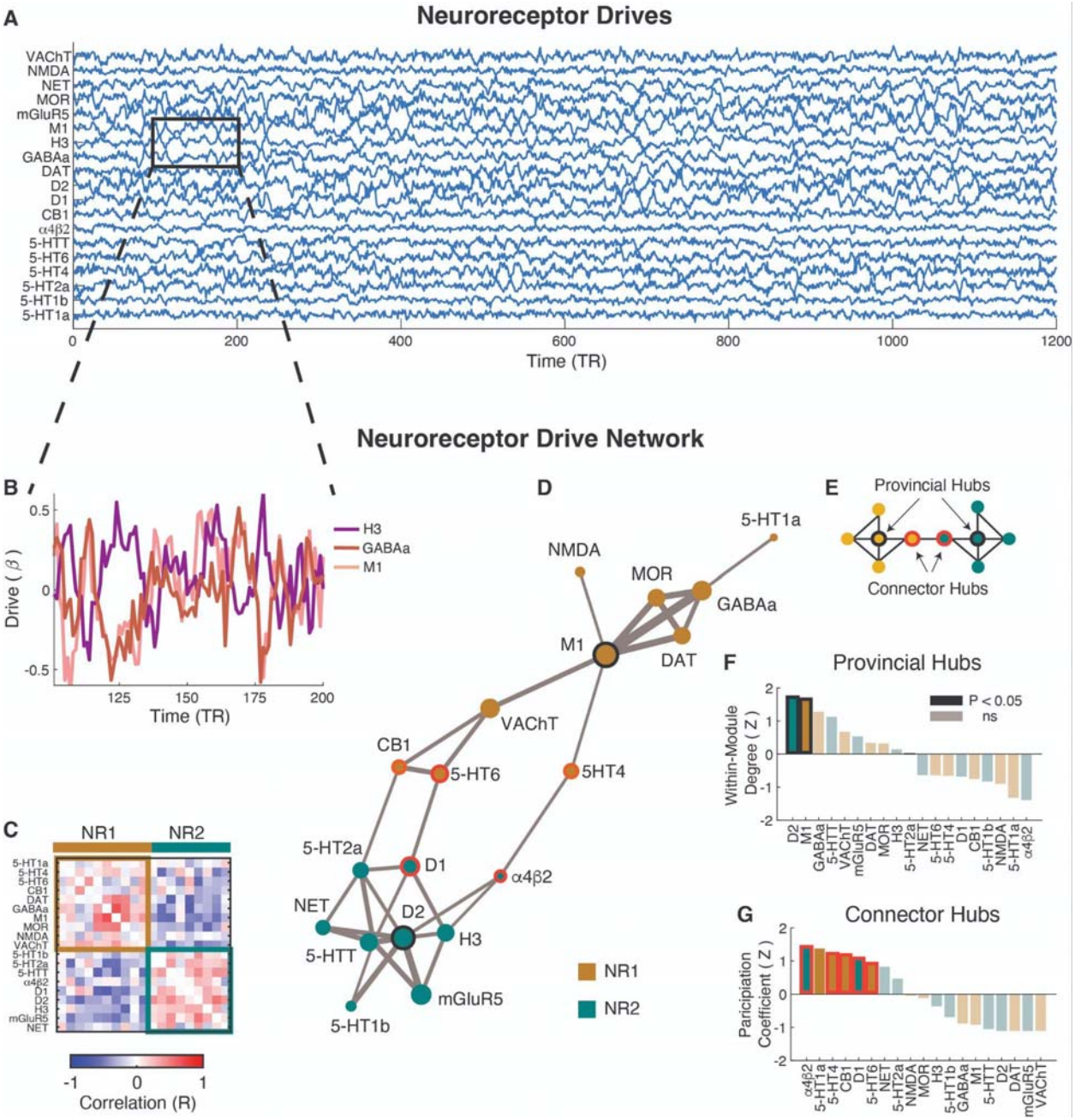

Figure 2. Two neuroreceptor and transporter modules underlie spontaneous brain activity. (A) Drive values (β-values) for all 19 neuroreceptors and transporters from a representative participant. (B) Drive values for GABAa, M1, and H3 neuroreceptors over a period of time from the same participant. (C) Group-level drive network depicting the strength of coordination between neuroreceptor drive values over time. Drive network was estimated using Pearson correlation to quantify the extent of pairwise coordination among neuroreceptors and transporters over time. Clustering analysis identified two distinct modules, NR1 and NR2. (D) Visualization of the drive network structure, showing only the top 20% of strongest connections. Node size indicates the weighted degree of the network, while edge thickness reflects the strength of connections (R-value) between neuroreceptors. The black outline represents provincial hubs, and the red outline represents connector hubs. (E) Schematic representation of provincial and

connector hubs in a network. (F) Provincial hub and (G) connector hub scores for each neuroreceptor, ranked according to hub score. Hub scores were calculated using positive values in the neuroreceptor drive network, and statistical significance was assessed by permuting the drive network in Panel C 1,000 times. Outlined bars represent identified hubs. Note that while 5-HT1a exhibited a high connector hub score, it was not considered a hub due to weak correlation values within and between modules. ns, non-significant.

To quantify the extent of coordination among neuroreceptors and transporters, the drive values were concatenated across participants and pairwise coordination was estimated using Pearson correlation. Positive correlations indicated coordinated changes, as observed between GABAa and M1 ($R_{GABAa:M1} = 0.68$), while negative correlations suggested inverse relationships, such as between GABAa and H3 ($R_{GABAa:H3} = -0.29$). Across all neuroreceptors and transporters, the correlations form a neuroreceptor drive network representing the overall coordination among all neuroreceptors and transporters. Additionally, clustering this network could reveal whether the observed coordination between GABAa and M1 suggests the existence of modules comprised of multiple neuroreceptors and transporters working in concert.

The neuroreceptor drive network revealed distinct patterns of positive and negative correlations among drive values, consistent with those observed between GABAa, M1, and H3 (**Fig. 2C,D**). Moreover, clustering analysis identified two distinct modules, NR1 and NR2 of neuroreceptors and transporters. Additionally, as shown in Figure 2D, a subset of neuroreceptors within both the NR1 and NR2 modules exhibited strong coordination with other neuroreceptors in their respective modules (back outlined nodes), while another subset acted as connectors linking the NR1 and NR2 modules (red outlined nodes).

Neuroreceptors or transporters that showed strong coordination (i.e., positive correlations) within their module are referred to as provincial hubs, whereas those linking different modules are termed connector hubs (**Fig. 2E**). To quantify the role of a neuroreceptor or transporter as a provincial hub, we calculated the within-module degree, which measures the strength of coordination within the same module. The M1 neuroreceptor was identified as a candidate provincial hub in the NR1 module, while the D2 neuroreceptor was identified as a candidate provincial hub in the NR2 module ($P_{perm} < 0.05$; **Fig. 2F**). In contrast, the participation

coefficient was used to quantify the role of neuroreceptors and transporters as connector hubs linking the NR1 and NR2 modules. The top candidate connector hubs identified were α4β2, 5-HT4, 5-HT6, CB1, and D1 ($P_{perm} < 0.05$; **Fig. 2G**). Additionally, the neuroreceptor drive network retained the same organization (R = 0.93) even after accounting for spatial similarity among neuroreceptor and transporter density maps (**Fig. S2**).

Notably, the NR1 and NR2 modules were not defined by neuromodulator families or by excitatory versus inhibitory properties. Instead, we observed distinct density distributions of these modules across the cortex (**Fig. 3**). The average density of neuroreceptors and transporters in both NR1 and NR2 was highest in the inferior prefrontal regions, insula, and temporal areas (**Fig. 3A,B**). However, NR2-associated neuroreceptors and transporters showed greater density in the frontal, motor, and visual cortices, while the NR1 module was more prominent in the orbitofrontal, parietal and temporal regions (**Fig. 3C**). Together, these findings indicate that coordinated interactions among diverse neuromodulators, neuroreceptors, and transporters contribute to the shaping of emergent patterns in brain activity.

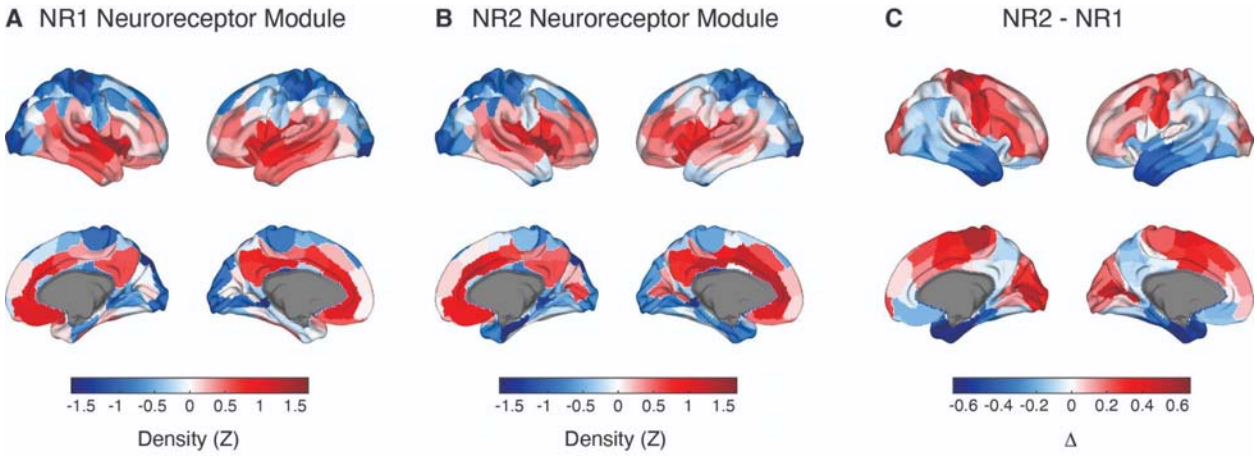

Figure 3. Cortical density differences between neuroreceptor modules. (A) The average density of the neuroreceptors and transporters part of the NR1 module. Module density map was estimated by averaging the z-score normalized neuroreceptor and transporter density maps part of the NR1 module. See Figure S1 for individual neuroreceptor and transporter density maps. (B) Same as panel A, but for the NR2 module. (C) Difference in the density across the cortex between the NR1 and NR2 modules. NR2-associated neuroreceptors and transporters exhibited greater density in the frontal, motor, and visual cortices, while the NR1 module was more prominent in the orbitofrontal, parietal and temporal regions.

Validating the neurobiological association between density maps and BOLD activity

Merely demonstrating that the BOLD signal can be reconstructed from neuroreceptor and transporter density maps is insufficient to establish that the underlying relationship genuinely reflects neurobiological associations. This limitation highlights the necessity of validating whether the analysis captures genuine neurobiological associations. In humans, such validation can be achieved by assessing whether the analysis can accurately reflect alterations in brain activity induced by neuropharmacological agents. The critical aspect of this validation involves determining whether the analysis can successfully identify the neuroreceptors and transporters known to mediate the effects of a given neuropharmacological agent. Successfully recovering these known neuroreceptors would provide strong support that the identified relationship between the BOLD signal and the neuroreceptors and transporters truly reflects the underlying neurobiological mechanism.

We utilized two datasets in which participants received LSD and Modafinil to validate that the reconstructed BOLD activity from neuroreceptor and transporter density maps accurately reflects neurobiological associations. In the first dataset, participants (N = 15) underwent 7 minutes of resting-state fMRI after receiving a Placebo and LSD[30]. In the second dataset, participants (N = 13) underwent 5 minutes of resting-state fMRI scanning before and after receiving Modafinil[31]. Moreover, understanding the mechanism of action of these drugs is important because they have been shown to exhibit beneficial effects for the treatment of neurological and neuropsychiatric disorders[32,33].

Focusing first on the LSD dataset, the BOLD signal and the functional connectivity were reconstructed in the same manner as was done in the HCP dataset. We first established using the data after administration of the Placebo that the neuroreceptor-based framework reconstructed the BOLD signal significantly greater than both null models ($R_{BOLD} = 0.68 \pm 0.02$; $P_{spatial} < 0.001$; $P_{spin} < 0.001$) as well as the functional connectivity ($R_{FC} = 0.64$; $P_{spatial} < 0.001$; $P_{spin} < 0.001$) (**Fig. S3A-C**). Similar results were obtained after the administration of LSD for both the BOLD signal ($R_{BOLD} = 0.66 \pm 0.02$) and functional connectivity ($R_{FC} = 0.63$; $P_{spatial} < 0.001$; $P_{spin} < 0.001$; **Fig. S3D-F**). The model reconstructed the temporal BOLD signal significantly better

after administration of the Placebo compared to LSD (t = 2.82, P = 0.01), but these differences were relatively small (ΔR_{ave} = 0.02; **Fig. S3G**). Moreover, the neuroreceptor-based framework reconstructed the empirical changes in functional connectivity between the LSD and Placebo conditions estimated using edgewise paired sample t-test significantly greater than both null models ($R_{LSD\text{-}Placebo}$ = 0.38; $P_{spatial}$ < 0.001; P_{spin} < 0.001; **Fig. S3H,I**). Together, these findings confirm the findings that the neuroreceptor-based framework is able to reconstruct the multiple facets of the BOLD signal and functional connectivity.

The critical element in the validation analysis is to determine the neuroreceptor(s) and transporter(s) altering the neuroreceptor drive network and correspondingly the brain activity from the state before to the state after administration of a neuropharmacological agent. The first step to determining the mechanism of action is to estimate the neuroreceptor drive networks D_p and D_q for brain *state p* and *state q*, which can correspond to the state before and the state after administration of LSD or Modafinil (**Fig. 4A**). Importantly, D_p and D_q dictate the extent of coordination among neuroreceptors and transporters driving brain activity. Therefore, changes in the drive network will correspondingly be reflected in the BOLD signal. We propose that the transition from state *p* to state *q* is mediated by a modulation network, *M*, that shifts the drive network from D_p to D_q. Mathematically, this is formulated as:

$$D_q = D_p \bullet M \qquad (1)$$

and *M* can be determined by taking the inner product between the inverse of D_p and D_q:

$$M = inv\left(D_p\right) \bullet D_q \qquad (2)$$

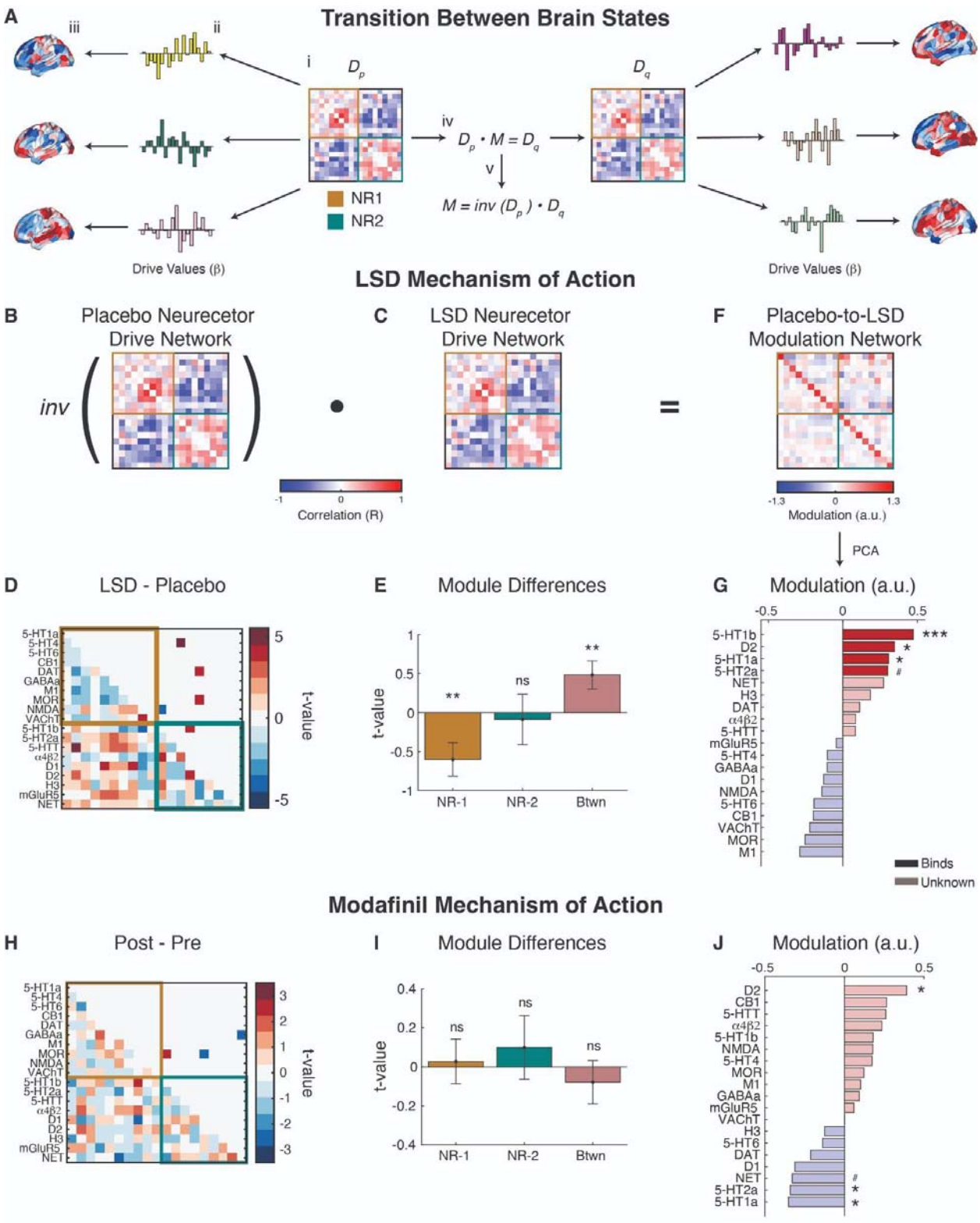

Figure 4. Neuroreceptor-based framework identifies the neuroreceptors and transporters mediating the effects of LSD and Modafinil. (A) Schematic representation of transition between brain states. (i) The neuroreceptor drive network, D_p, (ii) dictates the extent to which

individual neurochemicals acting through their receptors contribute to (iii) brain activity. (iv) The transition between brain states, such as before to after administration of a neuropharmacological agent is mediated by a modulation network, *M*, that shifts the drive network from D_p to D_q. (v) *M* can be determined by taking the inner product between the inverse of D_p and D_q. Critically, all diagonal elements in the neuroreceptor drive networks are set to zero. Panel A is only for illustrative purposes and formal analyses are shown in panels B-J. (B-G) Mechanism of action of LSD. (B) Group-level neuroreceptor drive network after placebo administration, estimated from the drive values from each of the 19 neuroreceptor and transporter using Pearson correlation. Group-level neuroreceptor drive network is estimated by averaging the neuroreceptor drive network across participants. The network is organized according to the module organization identified in the HCP dataset. (C) Same as panel B, but after administration of LSD. (D) Differences between the LSD and placebo drive networks, assessed using paired samples t-tests. Correlation values were Fisher z-transformed prior to statistical testing. The top half of the network shows statistically significant changes ($P < 0.05$, FDR corrected), while the bottom half illustrates the magnitude of all pairwise changes. (E) Changes in drive network connectivity within and between (Btwn) modules, evaluated using a one-sample t-test to determine significant deviations from zero. (F) Group-level modulation network driving the shifts in brain activity from the placebo to the LSD-induced brain state. Modulation network is estimated by taking the inner product between the inverse of Placebo (panel B) and LSD Neuroreceptor drive network (panel C). (G) The first principal component of the modulation network to determine the extent of modulation induced by each neuroreceptor and transporter in driving the transition from the placebo to LSD state. (H-J) Mechanism of action of Modafinil. Same as panel D, E, and G, but for Modafinil. ***$P < 0.001$; **$P < 0.01$; *$P < 0.05$; $^{\#}P < 0.1$; ns, not significant.

To apply the mathematical framework to the LSD dataset, we first estimated the corresponding neuroreceptor drive network after administration of the Placebo and LSD (**Fig. 4B,C**). The neuroreceptor drive network exhibited only a small number of significant pairwise changes in response to LSD ($P_{FDR} < 0.05$; **Fig. 4D**). These alterations were part of broader shifts within and between modules indicating significant decreases in coordination among the neuroreceptors part of the NR1 module ($t_{ave} = -0.60 \pm 1.45$; $P = 0.01$) and a shift toward enhanced coordination between modules ($t_{ave} = 0.48 \pm 1.71$; $P = 0.01$; **Fig. 4E**).

The neuroreceptors and transporters inducing these changes in the neuroreceptor drive network are reflected in the modulation network. As can be observed in Figure 4F, the modulatory network indicated that LSD exerted a complex set of changes affecting most relationships across the neuroreceptor drive network. To determine the neuroreceptors primarily responsible for the modulations, Principal Component Analysis (PCA) was used to identify the dominant

constituents underlying *M*. The first principal component of the modulatory network accounted for 35.89% ($P_{perm} < 0.001$) of the variance and all other components were not significant ($P_{perm} > 0.05$; **Fig. S4A**). The neuroreceptor primarily responsible for driving LSD induced changes in brain activity was 5-HT1b ($P_{perm} = 7.2 \times 10^{-4}$), followed by D2 ($P_{perm} = 0.01$), 5-HT1a ($P_{perm} = 0.03$) and 5-HT2a ($P_{perm} = 0.07$; **Fig. 4G**). These neuroreceptors are known to bind LSD, with 5-HT1b in particular having the highest affinity for LSD[34].

Extending the analysis to Modafinil, the model accurately reconstructed the BOLD signal and functional connectivity *pre* ($R_{BOLD} = 0.59 \pm 0.03$; $R_{FC} = 0.62$; $P_{spatial} < 0.001$; $P_{spin} < 0.001$) and *post* administration of Modafinil ($R_{BOLD} = 0.60 \pm 0.03$; $R_{FC} = 0.66$; $P_{spatial} < 0.001$; $P_{spin} < 0.001$; **Fig. S5A-F**). Additionally, the analysis reconstructed equally well both the brain activity *pre* and *post* administration of Modafinil ($t = -1.34$, $P = 0.20$) and the reconstructed functional connectivity reflected the observed differences between *pre* and *post* Modafinil ($R_{Post\text{-}Pre} = 0.37$; $P_{spatial} < 0.001$; $P_{spin} < 0.001$; **Fig. S5G-I**). Significant pairwise differences in the neuroreceptor drive network were found ($P < 0.05$; **Fig. 4H**; **Fig S5J,K**), but no significant differences were observed within and between the NR1 and NR2 modules ($P > 0.05$; **Fig. 4I**).

The modulation network indicated that Modafinil mediated effects were driven by a subset of neuroreceptors and transporters (**Fig. S5L**). The first PCA component which accounted for 99.02% ($P_{perm} < 0.001$; **Fig. S4B)** of the variance in the modulation network indicated that Modafinil mediated effects were primarily driven by D2 ($P_{perm} = 0.02$), followed by 5-HT1a ($P_{perm} = 0.03$), 5-HT2b ($P_{perm} = 0.05$), and NET ($P_{perm} = 0.07$; **Fig. 4J**). The exact mechanism of action of Modafinil is not known, but these results align with prior work showing that Modafinil alters dopamine and serotonin levels in the brain[35–38]. Correctly identifying known neuroreceptors that bind LSD and those mediating the effects of Modafinil indicated that the underlying relationship between the BOLD signal and neuroreceptor and transporter density map could reveal the mechanism of action of neuropharmacological agents, and the observed relationship genuinely reflects neurobiological processes validating the relevance of the proposed framework.

<u>Neuroreceptors inducing neuropsychiatric illness induces changes in the BOLD signal</u>

We then investigated whether this framework could be extended to provide a mechanistic relationship between the neuroreceptors, transporters and neuropsychiatric illnesses. Linking neuropsychiatric illnesses to specific neuroreceptors, transporters or neuromodulators is critical since it would improve diagnosis and treatment. For this analysis, we used the UCLA Consortium for Neuropsychiatric Phenomics (LA5c) dataset, which includes individuals diagnosed with schizophrenia (N = 45), bipolar disorder (N = 36), and attention deficit/hyperactivity disorder (ADHD; N = 39), along with a healthy control group (N = 118)[39].

To identify the neuroreceptors and transporters associated with schizophrenia, bipolar disorder, and ADHD, we applied the same framework used to determine the mechanism of action of LSD and Modafinil. We reconstructed the temporal BOLD signal for each participant using the 19 neuroreceptor and transporter density maps. The reconstruction accuracy of the healthy control group (R_{BOLD} = 0.55 ± 0.01; mean ± SEM) was not significantly different from the schizophrenia (R_{BOLD} = 0.55 ± 0.01; $P_{Diff_SCZ_to_HC}$ = 0.80), bipolar disorder (R_{BOLD} = 0.55 ± 0.02; $P_{Diff_BD_to_HC}$ = 0.08), and ADHD groups (R_{BOLD} = 0.55 ± 0.01; $P_{Diff_ADHD_to_HC}$ = 0.43; **Fig. S6**). Additionally, the neuroreceptor-based framework reconstructed differences in functional connectivity between neuropsychiatric groups and healthy controls significantly greater than null models for schizophrenia ($R_{SCZ\text{-}HC_FC}$ = 0.56; $P_{spatial}$ < 0.001; P_{spin} < 0.001), bipolar disorder ($R_{BD\text{-}HC_FC}$ = 0.45; $P_{spatial}$ < 0.001; P_{spin} < 0.001), and ADHD ($R_{ADHD\text{-}HC_FC}$ = 0.35; $P_{spatial}$ < 0.001; P_{spin} < 0.001; **Fig. S7**). These findings further support the effectiveness of neuroreceptor and transporter density maps in reconstructing spontaneous brain activity.

In the schizophrenia group, the neuroreceptor drive network exhibited a limited number of significant pairwise changes compared to healthy controls (P < 0.05) and these changes were part of a broader set of alterations within and between neuroreceptor drive network modules (P < 0.05; **Fig. S8A**). To determine the neuroreceptors and transporters driving these changes, we estimated the modulation network required to transition from the healthy to the schizophrenic brain state in the same manner as the analysis on LSD and Modafinil. The modulation network exhibited a complex pattern, with the first principal component accounting for 67.65% of the variance (P_{perm} < 0.001); all other components were not significant (P_{perm} > 0.05; **Fig. S8B**). The modulation analysis identified norepinephrine transporter (NET) as the primary driver (P_{perm} =

0.02; **Fig. 5A**). Other neuroreceptors mediating the effects included serotonin receptors 5-HT1a (P_{perm} = 0.03) and 5-HT4 (P_{perm} = 0.09), and additional associations with NMDA (P_{perm} = 0.02), α4β2 (P_{perm} = 0.07), and GABAa (P_{perm} = 0.09) neuroreceptors.

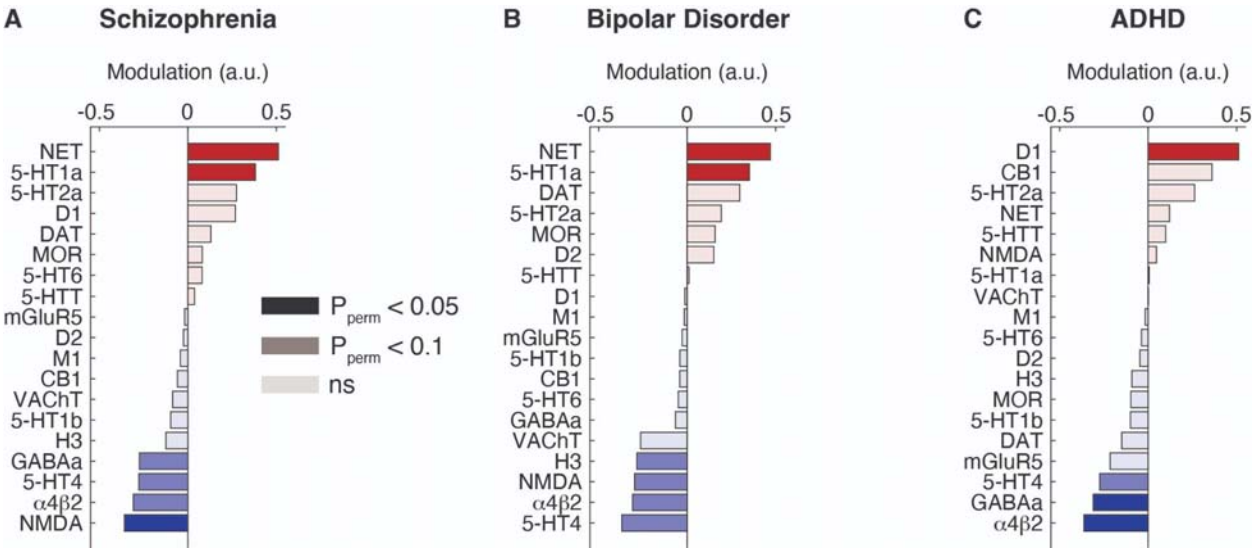

Figure 5. Neuroreceptors and transporters mediating the alterations in brain activity across neuropsychiatric disorders. (A) Neuroreceptors and transporters mediating the changes in brain activity from healthy controls (HC) to schizophrenia (SCZ). (B,C) Same as panel A, but for bipolar disorder (BD) and ADHD, respectively. Statistical significance was determined based on a permutation test and $P_{perm} < 0.05$ were considered significant. ns, not significant.

For bipolar disorder and ADHD, the analysis similarly identified a small set of pairwise changes within and between neuroreceptor network modules ($P < 0.05$; **Fig. S8C-F**). In bipolar disorder, NET was the primary driver similar to schizophrenia (P_{perm} = 0.04; **Fig. 5B**). Overall, neuroreceptor mediating the effect of bipolar disorder included 5-HT1a (P_{perm} = 0.01), 5-HT4 (P_{perm} = 0.06), α4β2 (P_{perm} = 0.07), NMDA (P_{perm} = 0.08), and H3 histamine (P_{perm} = 0.09) neuroreceptors. In ADHD, changes were mediated by the dopamine, D1 (P_{perm} = 0.01), and acetylcholine, α4β2 (P_{perm} = 0.01) neuroreceptors (**Fig. 5C**). The analysis also implicated GABAa (P_{perm} = 0.04) and the 5-HT4 serotonin neuroreceptor (P_{perm} = 0.07). Overall, findings suggest that these disorders may involve dysregulation across multiple neuromodulators and/or neuroreceptor and transporter systems.

<u>Subject-specific neuroreceptors driving neuropsychiatric induced alterations in the BOLD signal</u>

Neuropsychiatric disorders exhibit considerable variability at the individual level in their relationships with the brain[40,41]. A critical question is whether this variability can be attributed to specific neuroreceptors and transporters unique to each patient. To explore this, we extended our framework for identifying neuroreceptors driving group-level alterations in brain activity to individual patients. Using a patient-specific framework, we identified the neuroreceptors and transporters responsible for shifting brain activity from a healthy state to one associated with neuropsychiatric illness in each patient. Additionally, we assessed whether the extent of modulation by individual neuroreceptors formed distinct subgroups of patients with shared profiles.

For the schizophrenia, bipolar disorder, and ADHD cohorts, the analysis identified three subgroups of patients with distinct neuroreceptors and transporters driving the changes (**Fig. S9**). Moreover, we tested if subgroups could be identified from the functional connectivity profile estimated from the BOLD signal. Clustering individuals based on their functional connectivity profile did not identify clear subgroups or differences in the modulation values across neuroreceptors and transporters in schizophrenia, bipolar disorder or ADHD ($P > 0.05$; **Fig. S10**). Collectively, these findings suggest that the neuroreceptor-based framework could be a new avenue for personalized diagnostics and tailored therapeutic interventions.

<u>Consistent neuroreceptor drive networks across datasets</u>

Further, we assessed the similarity of neuroreceptor drive networks across datasets. Strong similarity between these independent datasets would enhance the validity. To quantify the extent of similarity, we compared the neuroreceptor drive networks derived from the LSD, modafinil, and LA5c datasets to the network estimated from the HCP dataset. Neuroreceptor drive networks from each of the other datasets showed strong similarity with the HCP-derived network (R_{ave} = 0.92; **Fig. S11**). This consistent relationship between the BOLD signal and neuroreceptors and transporters across diverse conditions underscores the stable dynamical interplay between brain activity and the underlying neuromodulator, neuroreceptors and transporters.

<u>Reconstructing spontaneous brain activity: neuroreceptors vs. structural and geometric modes</u>

Lastly, previous work has shown that spontaneous brain activity is shaped and constrained by anatomical factors – structural connectivity (SC)[42,43] and cortical folding geometry (GC)[44]. Models based on SC and GC suggest that spontaneous brain activity emerges from a weighted linear summation of modes (also called harmonics) of the SC or GC. However, it is an open question as to which model – neuroreceptor, structural or geometric – can accurately and parsimoniously reconstruct spontaneous brain activity.

Toward this end, we compared the accuracy of the neuroreceptor-based reconstructed maps of the dominant spatial patterns of the BOLD signal with reconstructed maps obtained using structural and geometric modes. For this analysis, we utilized the BOLD signal from the HCP dataset due to its extensive scanning duration. Specifically, the BOLD signal was concatenated across participants resulting in 200 x 57,600 data points. PCA was applied to the concatenated BOLD signal to identify the dominant spatial patterns of activity. We focus on the first three components – C1, C2, and C3 – which accounted for 23.57% of the variance to demonstrate the differences in reconstruction accuracy between neuroreceptor-, structural- and geometric-based frameworks (**Fig. 6A**). The neuroreceptor-based reconstructed components closely matched the empirical components with high accuracy ($R_{C1} = 0.73$; $R_{C2} = 0.64$; $R_{C3} = 0.85$; **Fig. 6B**). The accuracy was significantly greater than that observed in null models ($P_{spatial} < 0.001$; $P_{spin} < 0.001$; **Fig. 6C**).

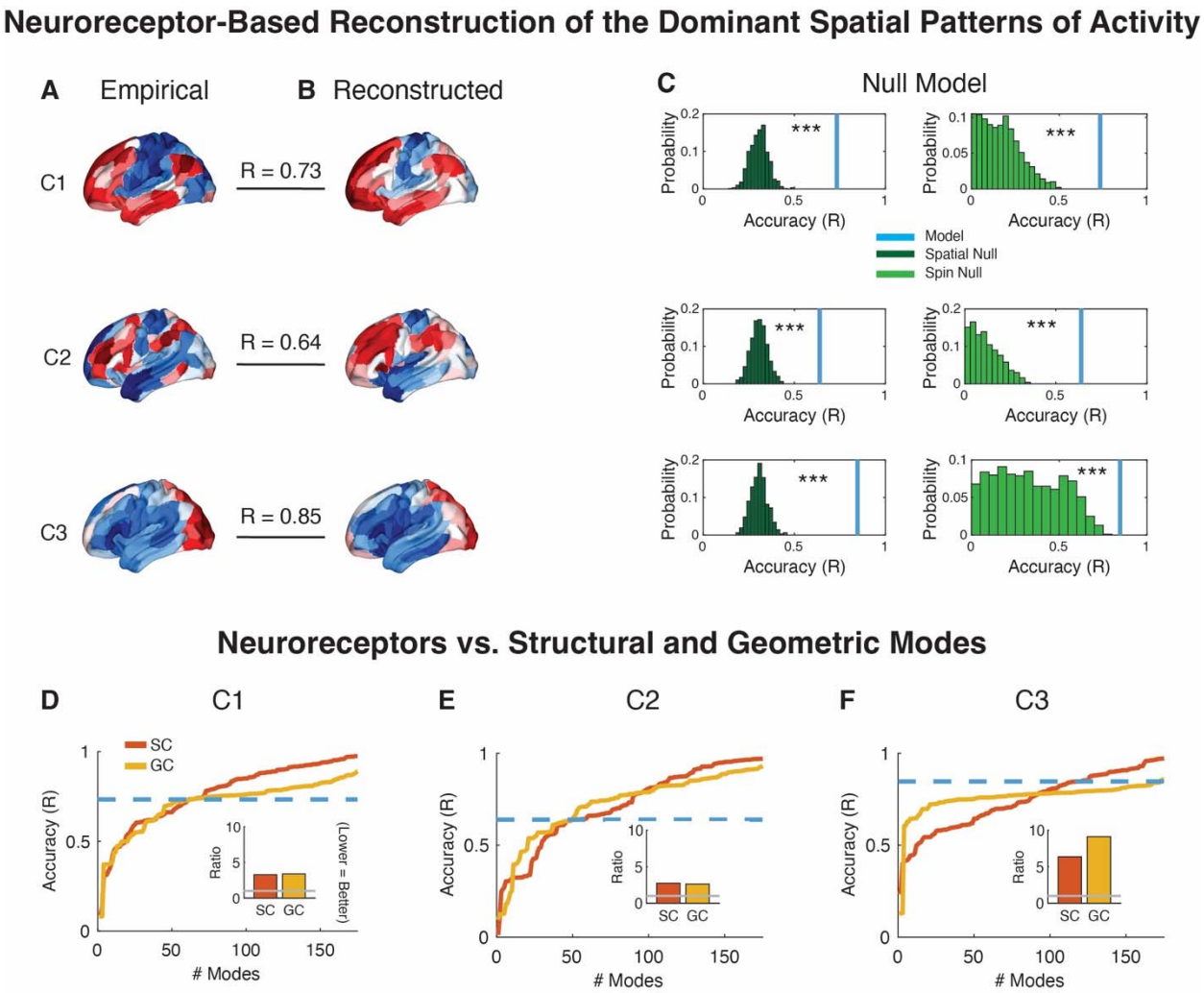

Figure 6. Neuroreceptor-based reconstruction outperforms models based on structural and geometric modes. (A) Brain maps of the dominant spatial patterns of the BOLD signal identified using PCA – C1, C2, and C3. (B) Neuroreceptor-based reconstruction accuracy of the BOLD components C1, C2, and C3. Accuracy was estimated using Pearson correlation. (C) Comparison with two null models: spatially permuted (*left*) and spin permutation (*right*). The blue line indicates the accuracy of the neuroreceptor-based reconstruction from panel B. (D-F) The number of structural and geometric modes required to achieve the same reconstruction accuracy as the neuroreceptor-based framework for BOLD signal components (D) C1, (E) C2, and (F) C3. The blue line represents the reconstruction accuracy obtained using neuroreceptors and transporters, as shown in panel B. The insert plot shows the ratio of the number of structural and geometric modes to the 19 neuroreceptors and transporters. The gray line indicates parity. ***P < 0.001.

SC and GC-based reconstruction was based on the method proposed by Pang *et. al.*, in which modes were sequentially added to the model until the reconstruction accuracy of the SC- and

GC-based frameworks equaled the accuracy obtained with the neuroreceptor-based framework[44]. SC or GC based reconstructions were deemed to outperform if fewer modes were required to achieve the save accuracy as the neuroreceptor-based framework. For BOLD components C1, C2, and C3, the SC-based reconstruction required at least 52 modes, while the GC-based reconstruction required at least 50 modes to match the accuracy achieved by using only 19 neuroreceptor and transporter density maps—demonstrating the effectiveness of reconstructing spontaneous brain activity with neuroreceptor density maps (**Fig. 6D-F**).

The analysis was extended to include components C4 through C10 which account for a total 40.85% of variance to corroborate the findings on components C1, C2 and C3. The neuroreceptor-based framework accurately reconstructed these additional components with an accuracy of $R > 0.64$, significantly exceeding both null models ($P_{spatial} < 0.001$; $P_{spin} < 0.001$; **Fig. S12**). Reflecting the findings with components C1, C2 and C3, the neuroreceptor-based reconstruction was more parsimonious for 8 out of the 10 BOLD components (**Fig. S13**). Only components C4 and C6 required fewer GC modes than the neuroreceptor analysis. However, these components accounted for only 4.01% and 2.57% of the spatiotemporal variance in the BOLD signal, respectively. The parsimony of the neuroreceptor-based framework in reconstructing spontaneous brain activity suggests that neuroreceptor and transporters may provide a more direct and biologically meaningful basis for modeling brain function compared to anatomical-based approaches.

Discussion

Neuromodulators are the primary substrate by which neurons communicate[45]. Like most aspects of the human brain, no individual neuromodulator works alone to generate brain activity; instead brain activity is generated from coordination among multiple neuromodulators acting through their corresponding neuroreceptors and transporters[2]. However, current methods provide limited insight[14], especially in humans [15] underscoring the need for a non-invasive framework to determine the neuromodulators driving brain activity. Here, we present a neuroreceptor-based framework that overcomes these limitations to identify the neuroreceptors and transporters working in congruence to drive spontaneous brain activity.

The neuroreceptor-based framework reconstructed the resting-state fMRI BOLD signal from a weighted linear summation of the spatial density maps from 19 neuroreceptors and transporters density maps estimated from PET imaging. The framework accurately reconstructed the BOLD signal and functional connectivity. Moreover, the analysis revealed the mechanism of action for an administered neuropharmacological agent – LSD and Modafinil. Further, the framework provided insight into the neuroreceptors and transporters inducing alterations in brain activity in schizophrenia, bipolar disorder and ADHD. Overall, reconstructing the BOLD signal from neuroreceptors and transporters density maps provides a non-invasive method to determine the neuroreceptors and transporters working in conjunction to drive brain activity at any given moment.

Spontaneous brain activity reflected a coordinated interplay among a diverse set of excitatory and inhibitory neuroreceptors and transporters, highlighting the complex neuromodulatory landscape of the cortex. Our findings suggest that the balance of excitation and inhibition is managed by two distinct modules – NR1 and NR2. The modules may serve as a safeguard against excessive excitation synchronization across cortical regions[46,47]. Moreover, the differing density distributions of neuroreceptors and transporters between modules across cortical regions suggests that brain activity and function is locally shaped by specific neuromodulatory profiles. For instance, the higher density of NR1 module in orbitofrontal, parietal and temporal areas may facilitate the integration of sensory and associative information[48], whereas the NR2 module's prominence in frontal, motor, and visual regions may align with the demand for rapid modulation of motor responses and visual processing[49,50]. This spatial organization suggests that the brain dynamically allocates neuromodulatory resources in a region-specific manner which may enhance its capacity to adapt to diverse cognitive and behavioral demands.

Why has the brain gone to such a great extent to maintain a rich tapestry of neuromodulators, neuroreceptors and transporters to facilitate communication? One possible reason could be that utilizing multiple neuromodulators, neuroreceptors and transporters could fine tune the excitation-inhibition balance, enabling neurons to maintain responsiveness across a broad spectrum of inputs and to adapt to varying inputs without changing their fundamental properties[51,52]. Furthermore, the interplay between different neuromodulators, neuroreceptors,

and transporters may serve an important role in network-level flexibility. We speculate that a brain region's capacity to respond to diverse neuromodulators enables it to be part of multiple subnetworks depending on the context. This versatility may facilitate efficient communication across the brain and support diverse cognitive functions without necessitating dedicated, fixed circuitry for every specific task[53]. Such a flexible integration among multiple subnetworks could allow the brain to maximize computational power while minimizing the metabolic costs[54].

The analysis also provided insight into the mechanism of action of an administered neuropharmacological agent. Determining the mechanism of action has been challenging because neuropharmacological agents have direct and indirect effects on the activation propensity of neuroreceptors and neurons[55]. The analysis accurately identified the neuroreceptors that bind LSD and neuroreceptors mediating the effects of Modafinil, providing strong support for the efficacy of the analysis. Showing that the analysis can identify the mechanism of action of LSD and Modafinil indicates that the framework could be utilized to provide insight into the mechanism of action of other neuropharmacological agents and narrow the search for therapeutic treatments for substance abuse[56,57] and neuropsychiatric illness[58,59].

We extended our framework to investigate neuropsychiatric disorders—schizophrenia, bipolar disorder, and ADHD—to identify the neuroreceptors and transporters driving alterations in brain activity associated with each condition. In both schizophrenia and bipolar disorder, the norepinephrine transporter (NET) emerged as a key mediator of dysfunction, aligning with prior pharmacological studies[60,61] and animal models[62] suggesting it plays a critical role in these conditions. The involvement of NET may reflect alterations in the Locus Coeruleus, a region responsible for the release of norepinephrine[63]. While the leading hypothesis and pharmacotherapy in schizophrenia is the dopamine hypothesis[64], however, medication targeting dopamine receptors exhibits limited efficacy[65,66]. In line with these findings, our results did not identify a significant association with dopamine neuroreceptors and transporters indicating that dopamine may not be the primary driver of schizophrenia. In bipolar disorder, norepinephrine is thought to play a role in triggering manic episodes[67]. For ADHD, the dopamine D1 neuroreceptor was identified as the primary driver of altered brain activity, consistent with previous research indicating its involvement in the disorder's pathophysiology[68]. Moreover, the

analysis identified the neuroreceptors and transporters underlying alterations in brain activity at the individual level indicating that the framework could be used for personalized diagnosis and treatment.

Our results suggest that these disorders may involve dysregulation across multiple neuromodulators and/or neuroreceptor and transporter systems rather than a single system. This across-the-board dysfunction could arise from an initial impairment in one system, with compensatory adjustments in others to maintain homeostasis[69]. Alternatively, a common underlying factor might disrupt multiple systems[70]. Alternatively, the observed dysfunction may reflect underlying abnormalities in the neurons responsible for releasing neurotransmitters such as norepinephrine or dopamine, with downstream effects manifesting in the associated neuroreceptors and transporters. This broad pattern of dysfunction highlights the complexity of neuropsychiatric conditions, underscoring the need for integrative approaches that consider the interplay among diverse neuromodulators. Toward this end, multimodal imaging can deepen our understanding of the coordinated roles of neuroreceptors and transporters in maintaining healthy brain function[71] and how their dysregulation can lead to pathological states[72,73].

The main focus of our analysis was on the relationship between neuroreceptors, transporters and the BOLD activity, but the BOLD signal can be reconstructed from anatomical factors – structural connectivity[42,43] and cortical folding geometry[44]. It is an open question as to which model – neuroreceptor, structural or geometric – accurately and parsimoniously reconstructs spontaneous brain activity. We found that the neuroreceptor model outperformed the alternatives suggesting that greater insight might be gained by shifting the focus from anatomical to neurochemical factors. Communication between brain regions and maintaining healthy brain states is reliant on anatomical factors and anatomical changes are associated with neuropathology, highlighting the importance of anatomical factors[74,75]. Nevertheless, the neuroreceptor-based framework outperformed the alternatives, suggesting it more effectively captures the relationship within and between brain regions. A neuroreceptor-based framework may be better at estimating brain activity since the concentration of neuroreceptors on dendritic spines can amplify signals from weak structural connections or diminish signals from strong physical connections estimated from diffusion MRI[76]. Additionally, brain regions that share

similar neuroreceptor and transporter profiles are more likely to exhibit similar patterns in brain activity since they would presumably respond to the same neuromodulators.

In summary, identifying the neuromodulators that drive brain activity is crucial due to their central roles in communication, cognition, and pathology, yet current in vivo detection methods are limited. Here, we demonstrated that these limitations can be overcome using cortical density maps of neuroreceptors and transporters from PET imaging. In the process, the framework revealed a complex network maintaining the excitation-inhibition balance. Further, this neuroreceptor-based framework can improve our ability to identify neuromodulators driving brain activity and opens new avenues for exploring dynamical brain activity, identifying neuropharmacological mechanisms of action and markers of neuropsychiatric disorders. Future studies can build on these findings to unravel the complex mechanisms that underlie cognition, and in generating targeted diagnostics and therapies.

Methods

Neuroreceptor Density Maps

The analysis used data originally published in Hansen *et al.*, 2022[24]. In brief, PET tracer imaging was used to map the density for 19 neuroreceptors and transporters. The neuroreceptors include 9 neurotransmitter systems: dopamine (D1, D2, DAT), norepinephrine (NET), serotonin (5-HT1A, 5-HT1B, 5-HT2A, 5-HT4, 5-HT6, 5-HTT), acetylcholine (α4β2, M1, VAChT), glutamate (mGluR5, NMDA), γ-aminobutyric acid (GABAa), histamine (H3), cannabinoid (CB1), and μ-opioid neuroreceptor (MOR). PET images were acquired only from healthy participants (n = 1,238; 718 males and 520 females). The images are used to estimate the binding potential and tracer distribution volume which are referred to as receptor densities. PET based estimation methods provide a direct measure of the neuroreceptor and transporter concentration across the cortex than estimates based on transcriptomics[77]. PET images were all registered to the MNI-ICBM 152 non-linear 2009 template and parcellated into the 200 regions according to the Schaefer atlas[25]. Finally, each map corresponding to individual neuroreceptors and transporters were z-score normalized.

Functional MRI Data

HCP Resting-State fMRI Dataset

We used pre-processed resting-state functional MRI (fMRI) data from 48 healthy human participants from the Human Connectome Project (HCP)[26]. We downloaded 50 participants, but two were missing data. In brief, participants underwent four sessions of 15-min resting-state scanning sessions. fMRI volumes were recorded using a customized 3T Siemens Connectome Skyra scanner with an EPI sequence (TR = 0.72 s, TE = 33.1 ms, 72 slices, 2.0 mm isotropic, field of view (FOV) = 208 × 180 mm). In addition to the pre-processing steps part of the HCP pipeline, we additionally regressed out the global signal, white matter, and cerebral spinal fluid. The data was mapped on Schaefer atlas to derive brain activity for 200 regions of interest because voxel-wise estimates can be unstable and noisy. Group-level functional connectivity (FC) was estimated using the Pearson correlation on the pooled data.

Lysergic Acid Diethylamide (LSD) Resting-State fMRI Dataset

The analysis was based on data detailed in Carhart-Harris *et. al.*, 2016[30]. In brief, the analysis utilized pre-processed fMRI data from 15 participants that underwent 7 minutes of resting-state fMRI after a placebo and LSD. fMRI data were acquired using a gradient echo planar imaging sequence, TR/TE = 2000/35ms, field-of-view = 220mm, 64 × 64 acquisition matrix, parallel acceleration factor = 2, 90° flip angle and 35 oblique axial slices and 3.4mm^3 voxel size.

Pre-processing steps are detailed in Carhart-Harris *et. al.*, 2016. fMRI data pre-processing involved de-spiking, slice time correction, motion correction, non-linear registration to 2mm MNI brain. Additionally, fMRI volumes with frame displacement greater than 0.4mm were removed. Finally, the functional data were spatially smoothed with a 6mm full-width half max kernel and band-pass filtering between 0.01 to 0.08 Hz. Finally, 9 nuisance regressors (6 motion-related and 3 were anatomically-related) and linear and quadratic trends were removed. Subject-level functional connectivity was estimated using the Pearson correlation.

Modafinil Resting-State fMRI Dataset

The analysis was based on data detailed in Cera *et. al.*, 2014[31]. In brief, the study recruited 26 young male right-handed (as assessed by the Edinburgh Handedness inventory) adults (age range: 25–35 y.o.). Participants received, in a double-blind fashion, either a single dose of Modafinil or a placebo pill identical to the drug. The present analysis focused only on 13 participants that received Modafinil.

Resting-state-fMRI BOLD data were separated in three runs lasting four minutes each followed by high resolution T1 anatomical images. BOLD functional imaging was performed with a Philips Achieva 3T Scanner (Philips Medical Systems, Best, The Netherlands), using T2*-weighted echo planar imaging (EPI) free induction decay (FID) sequences and applying the following parameters: TE 35 ms, matrix size 64×64, FOV 256 mm, in-plane voxel size 4×4 mm, flip angle 75°, slice thickness 4 mm and no gaps. 140 functional volumes consisting of 30 transaxial slices were acquired per run with a volume TR of 1671 ms. High resolution structural images were acquired at the end of the three rs-fMRI runs through a 3D MPRAGE sequence employing the following parameters: sagittal, matrix 256×256, FOV 256 mm, slice thickness 1 mm, no gaps, in-plane voxel size 1 mm×1 mm, flip angle 12°, TR = 9.7 ms and TE = 4 ms.

MRI data were preprocessed with the CONN Toolbox[78]. The preprocessed with the following steps: de-spiking, slice-timing correction, realignment, segmentation, coregistration, normalization, and spatial smoothing with 8 mm full width half maximum (FWHM). The preprocessing of the T1-weighted structural images involved skull-removal, normalization into MNI anatomical standard space, and segmentation into gray matter, white matter, and cerebral spinal fluid, soft tissues, and air and background. In functional images, all volumes with frame displacement greater than 0.3 mm were censored and followed by regression of the global signal.

UCLA Consortium for Neuropsychiatric Phenomics Dataset (LA5c)

The Consortium for Neuropsychiatric Phenomics includes imaging of healthy individuals (N=118 out of 122), individuals diagnosed with schizophrenia (N= 45 out of 50), bipolar disorder (N=35 out of 37), and attention deficit hyperactivity disorder (N= 39 out of 40)[39]. Resting-state functional MRI scans were obtained while participants kept their eyes open for 5 minutes in the scanner. Neuroimaging data were acquired on a 3T Siemens Trio scanner. T1-weighted high-resolution anatomical scans (MPRAGE) were collected with a slice thickness = 1mm, 176 slices, TR=1.9s, TE=2.26ms, matrix=256 x 256, FOV=250mm. Resting-state MRI data were collected with a T2*-weighted EPI sequence with slice thickness = 4mm, 34 slices, TR=2s, TE=30ms, flip angle=90°, matrix=64 × 64, FOV=192mm.

The analysis was based on minimally preprocessed data using FMRIPREP version 0.4.4 (http://fmriprep.readthedocs.io). T1-weighted volume was corrected for bias field using ANTs N4BiasFieldCorrection v2.1.0 skullstripped and coregistered ICBM 152 Nonlinear Asymmetrical template. Resting-state data were motion corrected using MCFLIRT v5.0.9. Functional data was skullstripped and coregistered to the corresponding T1-weighted volume using boundary-based registration. Motion correcting transformations, transformation to T1-weighted space and MNI template warp were applied in a single step using antsApplyTransformations. Framewise displacement and dvars were calculated using Nipype implementation. In addition to those regressors, global signal and mean white matter signal was also calculated and removed. Additionally, analysis was conducted only on participants with an average frame displacement less than 0.5 mm. In total the analysis was based on 118 out of 130

healthy controls, 45 out of 50 participants diagnosed with schizophrenia, 35 out of 49 participants diagnosed with bipolar disorder and 39 out of 43 participants diagnosed with ADHD. Moreover, in the remaining participants, all individual fMRI volumes with frame displacement greater than 0.3mm were removed. This dataset was chosen because it encompasses a diverse range of neuropsychiatric disorders while minimizing the potential measurement discrepancies that can occur when combining data from multiple sources.

Reconstructing BOLD Time Series, Components and Functional Connectivity from Neuroreceptor Density Maps

Reconstruction of the BOLD signal was conducted on both the timeseries and principal components of the BOLD signal. The same method was used for reconstructing the BOLD time series. Specifically, each of 1,200 fMRI volumes (time points) per participant were reconstructed from a weighted linear summation of the 19 neuroreceptor and transporter density maps. Formally, each volume of the BOLD signal is reconstructed as:

$$B_i = \beta_o + \sum_{j=1}^{19} \beta_j R_j \qquad (3)$$

where B_i is the ith BOLD volume. Further, R_j is the spatial density map associated with the jth neuroreceptor and transporter, β_o is the intercept and β_j is the estimated beta-values for each neuroreceptor map in the model. Model fitting was performed using *fitlm.m* in Matlab 2021b. Reconstruction accuracy of the BOLD signal was estimated using the Pearson correlation between empirical and reconstructed components.

Additionally, we determined if the neuroreceptor-based reconstruction of the BOLD timeseries preserved the inherent functional connectivity present in resting-state fMRI. To determine the accuracy in the functional connectivity of the reconstructed BOLD signal, the empirical and reconstructed BOLD signal was concatenated across participants and Pearson's correlation was used to estimate the functional connectivity, respectively.

The same framework was applied to the top ten BOLD spatial components in HCP dataset, LSD, Modafinil and LA5c datasets. For the component analysis, the BOLD data from all participants was pooled together resulting in 200 x 57,600 data points. Principal components of

the BOLD signal were identified using *pca.m* in Matlab 2021b. Consistent with the terminology used by Pang et al., 2023, we refer to this process as "reconstruction" to describe the estimation of BOLD activity from the model[44].

BOLD Reconstruction Null Models

Spatial Permutation Null Model

Reconstruction accuracy was compared to the spatial permutation null model. Specifically, for each of the 19 neuroreceptor and transporter density maps were spatially permuted and BOLD component and time series signal was reconstructed from the permuted maps. A total of 1000 permutations were conducted. Additionally, we estimated the functional connectivity from the reconstructed BOLD signal from the spatial null model by first concatenating the reconstructed BOLD signal estimated from the spatially permuted null model across participants and Pearson's correlation was used to estimate the functional connectivity. A total of 1000 permutations were performed and observed accuracy values greater than the spatial null model at a $P_{spatial} < 0.05$ were considered statistically significant.

Spin Null Model

Additionally, reconstruction accuracy was compared to the spin permuted null model[27]. Spin permutation, randomized each of the 19 neuroreceptor and transporter density maps but preserves the distance dependencies between brain regions. Similar to the spatial permutation null model, BOLD component and time series signal was reconstructed from the spin permuted maps. In the same manner as the spatial permutation null model, we estimated the functional connectivity from the reconstructed BOLD signal from the spin null model. A total of 1000 permutations were performed and observed accuracy values greater than the spin null model at a $P_{spin} < 0.05$ were considered statistically significant.

Neuroreceptor Drive Network Estimation and Network Properties

Estimating Neuroreceptor Drive Network

Neuroreceptor drive network was estimated by correlating the beta-values from the time series model. The neuroreceptor drive network was estimated from the pooled data across participants. Clustering of the neuroreceptor drive network was conducted using modularity-maximization[79].

Modularity-maximization does not require the number of clusters to be specified and the resolution of the clusters was controlled with resolution parameter, $\gamma = 1$. Modularity-maximization was implemented with the Generalized Louvain algorithm part of the Brain Connectivity Toolbox[80]. Clustering results from the Generalized Louvain algorithm can be dependent on the initial seeding. Therefore, clustering was repeated 100x with different initial seeds, and final clustering results were based on the consensus across iterations[81]. Specifically, consensus clustering identifies a single representative partition from the set of 100 iterations. This process involves the creation of a thresholded nodal association matrix which describes how often nodes were placed in the same cluster. The representative partition is then obtained by using a Generalized Louvain algorithm to identify clusters within the thresholded nodal association matrix.

Provincial Hubs

Provincial hubs are nodes in a network that have strong connection within a module[80]. A provincial hub score for each node was estimated using the within module degree which quantifies the strength of the connections a node exhibits with other nodes within a module. This involved first thresholding the network to remove all negative connections. Brain connectivity toolbox was used to estimate provincial hub scores[80]. Within-module z-score can me estimated as:

$$Z_i = \frac{k_i(m_i) - \underline{k}(m_i)}{\sigma^{k(m_i)}} \qquad (4)$$

where m_i is the module containing node i, $k_i(m_i)$ is the within-module degree of i, and $\underline{k}(m_i)$ and $\sigma^{k(m_i)}$ are the mean and standard deviation.

Connector Hubs

Connector hubs are nodes that link modules. A connector hub score was estimated for each node using participation coefficient (PC) as:

$$PC_i = 1 - \sum_{m \in M} \left(\frac{k_i(m)}{k_i}\right)^2 \qquad (5)$$

where M is the set of modules, and $k_i(m)$ is the strength of connection between i and all nodes in module m. As with the provincial hubs, the neuroreceptor network was first thresholded to

remove all negative connections. Brain Connectivity Toolbox was used to estimate participation coefficient and values were z-score normalized[80].

Statistical Testing of Hub Properties

Statistical significance for both provincial and connector hub scores was based on comparison to a null model. Specifically, a degree persevering permutation was utilized to randomize the neuroreceptor network prior to estimating the provincial and connector hub scores from the null model. A total of 1000 permutations were performed and empirical hub scores that were greater than the null model at a $P_{perm} < 0.05$ were considered statistically significant.

<u>Neuroreceptors Underlying LSD, Modafinil and Neuropsychiatric Illness Induced Changes</u>

To identify the neuroreceptors and transporters contributing to changes in brain activity following LSD, Modafinil, and in underlying neuropsychiatric conditions, we determined the neuroreceptors and transporters mediating these effects. The key analytical step involved identifying a modulatory network, *M*, that transforms the neuroreceptor drive network from state *p* to state *q*. The relationship can be expressed mathematically as:

$$D_q = D_p \bullet M \qquad (1)$$

Critically, all diagonal elements in *D* are set to zero ensuring that the neuroreceptor and transporter does not activate itself in the framework. M can be determined by solving:

$$M = inv\left(D_p\right) \bullet D_q \qquad (2)$$

The neuroreceptors driving the modulations can be identified by decomposing M using PCA. Moreover, the same analysis was used to gain insight into the neuroreceptor(s) and transporter(s) underlying Modafinil and neuropsychiatric illness.

The modulatory network, *M*, can fit any difference in the neuroreceptor drive networks even if the underlying differences are simply noise. Statistical significance was based on randomizing *M*, generating a random modulatory network, M_{rand} in a degree preserving manner. Randomizing the empirically derived *M* ensures that inherent properties such as the mean and standard deviation of *M* are preserved in M_{rand}. Once M_{rand} is estimated, it is decomposed using PCA and

the variance explained by each component is compared to *M*. The modulation values associated with each neuroreceptor, and transporter are compared. A total of 1000 permutations are performed and the principal component and neuroreceptors and transporters in the empirically derived *M* that deviate from M_{rand} at probability of $P_{perm} < 0.05$ are considered to be statistically significant.

<u>Model Comparison: Structural and Cortical Geometric Eigenmodes</u>

Structural Connectivity and Structural Eigenmodes

Preprocessed diffusion weighted images for each of the 48 participants part of the HCP were used to construct structural connectomes. Specifically, fiber tracking was done using DSI Studio with a modified FACT algorithm[82]. Data were reconstructed using generalized q-sampling imaging (GQI) in MNI space. Fiber tracking was performed until 250,000 streamlines were reconstructed with default parameters. For each participant, an undirected weighted structural connectivity matrix, A, was constructed from the connection strength based on the number of streamlines connecting two regions. Connectivity matrix was normalized by dividing the number of streamlines (T) between region *i* and *j*, by the combined volumes (*v*) of region *i* and *j*:

$$A_{ij} = \frac{T_{ij}}{v_i + v_j} \qquad (6)$$

Group structural connectivity was estimated by averaging all the individual structural connectivity networks together.

In accordance with Naze *et al.*, 2021, structural eigenmodes were estimated from the normalized graph Laplacian of the structural network as:

$$L = \frac{1}{2}[\,(D - A) + (D - A)^T] \qquad (7)$$

where *A* is the adjacency matrix of the group-level structural connectome and *D* is the degree matrix[83]. The graph Laplacian *L* is then decomposed into a finite number of eigenvalues λ_k and eigenvectors, ψ_k :

$$L\psi_k = \lambda\psi_k \qquad (8)$$

Cortical Geometric Eigenmodes

Cortical eigenmodes capture how the anatomy constrains brain dynamics. The analysis relies on cortical modes derived in Pang et. al., 2023[44]. In brief, cortical eigenmodes are estimated from the midthickness surface mesh part of the FreeSurfer's fsaverage population-averaged template. Local vertex-to-vertex spatial relations and curvature are modeled using the Laplace–Beltrami operator from the surface mesh, and from which the eigenmodes are estimated. Each eigenmode comprises spatial patterns with a specific wavelength.

Comparing Reconstruction Models

To compare the reconstruction models, we use the first 10 principal components of the BOLD signal. Specifically, each component is reconstructed using structural and geometric eigenmodes by sequentially adding modes to the model until the reconstruction accuracy of the models equals the accuracy obtained with the neuroreceptor-based model. Structural- or cortical geometric-based reconstructions were deemed to outperform if fewer modes were required to achieve the save accuracy as the neuroreceptor-based framework.

Data Availability

Minimally pre-processed Human Connectome Project data can be downloaded from https://www.humanconnectome.org/. Neuroreceptor composition data can be obtained at https://github.com/netneurolab/hansen_receptors. LSD dataset can be obtained at https://openneuro.org/datasets/ds003059/versions/1.0.0. Modafinil dataset can be obtained at https://openneuro.org/datasets/ds000133/versions/00001. UCLA Consortium for Neuropsychiatric Phenomics Dataset can be downloaded at https://openfmri.org/dataset/ds000030/. The brain connectivity toolbox can be downloaded at https://sites.google.com/site/bctnet/. Cortical geometric eigenmode data can be obtained at https://osf.io/xczmp/.

References

1. Hyman, S. E. Neurotransmitters. *Current Biology* **15**, R154–R158 (2005).
2. Shine, J. M. *et al.* Computational models link cellular mechanisms of neuromodulation to large-scale neural dynamics. *Nature Neuroscience* **24**, 765–776 (2021).
3. Luo, L. Architectures of neuronal circuits. *Science* **373**, 7285.
4. Deco, G. *et al.* How Local Excitation–Inhibition Ratio Impacts the Whole Brain Dynamics. *J. Neurosci.* **34**, 7886 (2014).
5. D'Esposito, M., Deouell, L. Y. & Gazzaley, A. Alterations in the BOLD fMRI signal with ageing and disease: a challenge for neuroimaging. *Nature Reviews Neuroscience* **4**, 863–872 (2003).
6. Reinen, J. M. *et al.* The human cortex possesses a reconfigurable dynamic network architecture that is disrupted in psychosis. *Nature Communications* **9**, 1157 (2018).
7. Durlauf, S. N. A framework for the study of individual behavior and social interactions. *Sociological Methodology* **31**, (2001).
8. Kable, J. W. & Glimcher, P. W. The neural correlates of subjective value during intertemporal choice. *Nature Neuroscience* **10**, (2007).
9. Afraz, A., Pashkam, M. V. & Cavanagh, P. Spatial heterogeneity in the perception of face and form attributes. *Current Biology* **20**, (2010).
10. Marvin, J. S. *et al.* An optimized fluorescent probe for visualizing glutamate neurotransmission. *Nature Methods* **10**, 162–170 (2013).
11. Sanfilippo, P. *et al.* Mapping of multiple neurotransmitter receptor subtypes and distinct protein complexes to the connectome. *Neuron* **112**, 942-958.e13 (2024).
12. Watson, C. J., Venton, B. J. & Kennedy, R. T. In Vivo Measurements of Neurotransmitters by Microdialysis Sampling. *Anal. Chem.* **78**, 1391–1399 (2006).
13. Bucher, E. S. & Wightman, R. M. Electrochemical Analysis of Neurotransmitters. *Annual Review of Analytical Chemistry* vol. 8 239–261 (2015).
14. Ou, Y., Buchanan, A. M., Witt, C. E. & Hashemi, P. Frontiers in electrochemical sensors for neurotransmitter detection: towards measuring neurotransmitters as chemical diagnostics for brain disorders. *Anal. Methods* **11**, 2738–2755 (2019).
15. Si, B. & Song, E. Recent Advances in the Detection of Neurotransmitters. *Chemosensors* **6**, (2018).
16. Rose, C. R. & Konnerth, A. NMDA Receptor-Mediated Na^+ Signals in Spines and Dendrites. *J. Neurosci.* **21**, 4207 (2001).
17. Yuste, R. & Denk, W. Dendritic spines as basic functional units of neuronal integration. *Nature* **375**, 682–684 (1995).
18. Hou, Z.-H. & Yu, X. Activity-regulated Somatostatin Expression Reduces Dendritic Spine Density and Lowers Excitatory Synaptic Transmission via Postsynaptic Somatostatin Receptor 4 *. *Journal of Biological Chemistry* **288**, 2501–2509 (2013).
19. Sander, C. Y., Hansen, H. D. & Wey, H.-Y. Advances in simultaneous PET/MR for imaging neuroreceptor function. *J Cereb Blood Flow Metab* **40**, 1148–1166 (2020).
20. Sander, C. Y. *et al.* Neurovascular coupling to D2/D3 dopamine receptor occupancy using simultaneous PET/functional MRI. *Proceedings of the National Academy of Sciences* **110**, 11169–11174 (2013).
21. Dipasquale, O. *et al.* Receptor-Enriched Analysis of functional connectivity by targets (REACT): A novel, multimodal analytical approach informed by PET to study the

pharmacodynamic response of the brain under MDMA. *NeuroImage* **195**, 252–260 (2019).
22. Salvan, P. *et al.* Serotonin regulation of behavior via large-scale neuromodulation of serotonin receptor networks. *Nature Neuroscience* **26**, 53–63 (2023).
23. Shine, J. M. *et al.* Human cognition involves the dynamic integration of neural activity and neuromodulatory systems. *Nature Neuroscience* **22**, 289–296 (2019).
24. Hansen, J. Y. *et al.* Mapping neurotransmitter systems to the structural and functional organization of the human neocortex. *Nature Neuroscience* **25**, 1569–1581 (2022).
25. Schaefer, A. *et al.* Local-Global Parcellation of the Human Cerebral Cortex from Intrinsic Functional Connectivity MRI. *Cerebral Cortex* **28**, 3095–3114 (2018).
26. Van Essen, D. C. *et al.* The WU-Minn Human Connectome Project: An overview. *NeuroImage* (2013) doi:10.1016/j.neuroimage.2013.05.041.
27. Alexander-Bloch, A. F. *et al.* On testing for spatial correspondence between maps of human brain structure and function. *NeuroImage* **178**, 540–551 (2018).
28. Thiele, A. & Bellgrove, M. A. Neuromodulation of Attention. *Neuron* **97**, 769–785 (2018).
29. Motley, S. E. Relationship Between Neuromodulation and Working Memory in the Prefrontal Cortex: It's Complicated. *Frontiers in Neural Circuits* **12**, (2018).
30. Carhart-Harris, R. L. *et al.* Neural correlates of the LSD experience revealed by multimodal neuroimaging. *Proceedings of the National Academy of Sciences* **113**, 4853–4858 (2016).
31. Cera, N., Tartaro, A. & Sensi, S. L. Modafinil Alters Intrinsic Functional Connectivity of the Right Posterior Insula: A Pharmacological Resting State fMRI Study. *PLOS ONE* **9**, e107145 (2014).
32. Ko, K., Kopra, E. I., Cleare, A. J. & Rucker, J. J. Psychedelic therapy for depressive symptoms: A systematic review and meta-analysis. *Journal of Affective Disorders* **322**, 194–204 (2023).
33. Erritzoe, D. *et al.* Exploring mechanisms of psychedelic action using neuroimaging. *Nature Mental Health* **2**, 141–153 (2024).
34. Ray, T. S. Psychedelics and the Human Receptorome. *PLOS ONE* **5**, e9019 (2010).
35. Volkow, N. D. *et al.* Effects of Modafinil on Dopamine and Dopamine Transporters in the Male Human Brain: Clinical Implications. *JAMA* **301**, 1148–1154 (2009).
36. Minzenberg, M. J. & Carter, C. S. Modafinil: A Review of Neurochemical Actions and Effects on Cognition. *Neuropsychopharmacology* **33**, 1477–1502 (2008).
37. Madras, B. K. *et al.* Modafinil Occupies Dopamine and Norepinephrine Transporters in Vivo and Modulates the Transporters and Trace Amine Activity in Vitro. *J Pharmacol Exp Ther* **319**, 561 (2006).
38. Qu, W.-M., Huang, Z.-L., Xu, X.-H., Matsumoto, N. & Urade, Y. Dopaminergic D_1 and D_2 Receptors Are Essential for the Arousal Effect of Modafinil. *J. Neurosci.* **28**, 8462 (2008).
39. Poldrack, R. A. *et al.* A phenome-wide examination of neural and cognitive function. *Scientific Data* **3**, 160110 (2016).
40. Winter, N. R. *et al.* Quantifying Deviations of Brain Structure and Function in Major Depressive Disorder Across Neuroimaging Modalities. *JAMA Psychiatry* **79**, 879–888 (2022).
41. Segal, A. *et al.* Regional, circuit and network heterogeneity of brain abnormalities in psychiatric disorders. *Nature Neuroscience* **26**, 1613–1629 (2023).
42. Atasoy, S., Donnelly, I. & Pearson, J. Human brain networks function in connectome-specific harmonic waves. *Nature Communications* **7**, 10340 (2016).
43. Atasoy, S., Deco, G., Kringelbach, M. L. & Pearson, J. Harmonic Brain Modes: A Unifying

Framework for Linking Space and Time in Brain Dynamics. *Neuroscientist* **24**, 277–293 (2018).
44. Pang, J. C. *et al*. Geometric constraints on human brain function. *Nature* **618**, 566–574 (2023).
45. Nadim, F. & Bucher, D. Neuromodulation of neurons and synapses. *Current Opinion in Neurobiology* **29**, 48–56 (2014).
46. Dasgupta, R., Seibt, F. & Beierlein, M. Synaptic Release of Acetylcholine Rapidly Suppresses Cortical Activity by Recruiting Muscarinic Receptors in Layer 4. *J. Neurosci*. **38**, 5338 (2018).
47. Lee, S., Kruglikov, I., Huang, Z. J., Fishell, G. & Rudy, B. A disinhibitory circuit mediates motor integration in the somatosensory cortex. *Nature Neuroscience* **16**, 1662–1670 (2013).
48. Dahl, C. D., Logothetis, N. K. & Kayser, C. Spatial Organization of Multisensory Responses in Temporal Association Cortex. *J. Neurosci.* **29**, 11924 (2009).
49. Zanto, T. P., Rubens, M. T., Thangavel, A. & Gazzaley, A. Causal role of the prefrontal cortex in top-down modulation of visual processing and working memory. *Nature Neuroscience* **14**, 656–661 (2011).
50. Narayanan, N. S. & Laubach, M. Top-Down Control of Motor Cortex Ensembles by Dorsomedial Prefrontal Cortex. *Neuron* **52**, 921–931 (2006).
51. Sweeney, Y., Hellgren Kotaleski, J. & Hennig, M. H. A Diffusive Homeostatic Signal Maintains Neural Heterogeneity and Responsiveness in Cortical Networks. *PLOS Computational Biology* **11**, e1004389 (2015).
52. Bharioke, A. & Chklovskii, D. B. Automatic Adaptation to Fast Input Changes in a Time-Invariant Neural Circuit. *PLOS Computational Biology* **11**, e1004315 (2015).
53. Cole, M. W. *et al.* Multi-task connectivity reveals flexible hubs for adaptive task control. *Nature Neuroscience* **16**, 1348–1355 (2013).
54. Bullmore, E. & Sporns, O. The economy of brain network organization. *Nature Reviews Neuroscience* **13**, 336–349 (2012).
55. Zhao, S. & Iyengar, R. Systems Pharmacology: Network Analysis to Identify Multiscale Mechanisms of Drug Action. *Annual Review of Pharmacology and Toxicology* vol. 52 505–521 (2012).
56. Tricklebank, M. D., Robbins, T. W., Simmons, C. & Wong, E. H. F. Time to re-engage psychiatric drug discovery by strengthening confidence in preclinical psychopharmacology. *Psychopharmacology* **238**, 1417–1436 (2021).
57. Khodosevich, K., Dragicevic, K. & Howes, O. Drug targeting in psychiatric disorders — how to overcome the loss in translation? *Nature Reviews Drug Discovery* **23**, 218–231 (2024).
58. Marder, S. R., Laughren, T. & Romano, S. J. Why Are Innovative Drugs Failing in Phase III? *AJP* **174**, 829–831 (2017).
59. Spark, D. L., Fornito, A., Langmead, C. J. & Stewart, G. D. Beyond antipsychotics: a twenty-first century update for preclinical development of schizophrenia therapeutics. *Translational Psychiatry* **12**, 147 (2022).
60. Borodovitsyna, O., Flamini, M. & Chandler, D. Noradrenergic Modulation of Cognition in Health and Disease. *Neural Plasticity* **2017**, 6031478 (2017).
61. Fitzgerald, P. J. Is elevated norepinephrine an etiological factor in some cases of schizophrenia? *Psychiatry Research* **215**, 497–504 (2014).
62. Siuta, M. A. *et al.* Dysregulation of the Norepinephrine Transporter Sustains Cortical

Hypodopaminergia and Schizophrenia-Like Behaviors in Neuronal Rictor Null Mice. *PLOS Biology* **8**, e1000393 (2010).

63. Mäki-Marttunen, V., Andreassen, O. A. & Espeseth, T. The role of norepinephrine in the pathophysiology of schizophrenia. *Neuroscience & Biobehavioral Reviews* **118**, 298–314 (2020).
64. Howes, O. D. & Kapur, S. The Dopamine Hypothesis of Schizophrenia: Version III—The Final Common Pathway. *Schizophrenia Bulletin* **35**, 549–562 (2009).
65. Howes, O. D., Bukala, B. R. & Beck, K. Schizophrenia: from neurochemistry to circuits, symptoms and treatments. *Nature Reviews Neurology* **20**, 22–35 (2024).
66. Correll, C. U. & Schooler, N. R. Negative Symptoms in Schizophrenia: A Review and Clinical Guide for Recognition, Assessment, and Treatment. *Neuropsychiatric Disease and Treatment* **16**, 519–534 (2020).
67. Kurita, M. Noradrenaline plays a critical role in the switch to a manic episode and treatment of a depressive episode. *Neuropsychiatric Disease and Treatment* **12**, 2373–2380 (2016).
68. Li, D., Sham, P. C., Owen, M. J. & He, L. Meta-analysis shows significant association between dopamine system genes and attention deficit hyperactivity disorder (ADHD). *Human Molecular Genetics* **15**, 2276–2284 (2006).
69. Davis, G. W. Homeostatic Signaling and the Stabilization of Neural Function. *Neuron* **80**, 718–728 (2013).
70. Borcuk, C. *et al.* Network-wide risk convergence in gene co-expression identifies reproducible genetic hubs of schizophrenia risk. *Neuron* doi:10.1016/j.neuron.2024.08.005.
71. Steel, A., Mikkelsen, M., Edden, R. A. E. & Robertson, C. E. Regional balance between glutamate+glutamine and GABA+ in the resting human brain. *NeuroImage* **220**, 117112 (2020).
72. Marín, O. Interneuron dysfunction in psychiatric disorders. *Nature Reviews Neuroscience* **13**, 107–120 (2012).
73. Vattikuti, S. & Chow, C. C. A Computational Model for Cerebral Cortical Dysfunction in Autism Spectrum Disorders. *Biological Psychiatry* **67**, 672–678 (2010).
74. Warren, D. E. *et al.* Network measures predict neuropsychological outcome after brain injury. *Proceedings of the National Academy of Sciences* **111**, 14247–14252 (2014).
75. van Erp, T. G. M. *et al.* Cortical Brain Abnormalities in 4474 Individuals With Schizophrenia and 5098 Control Subjects via the Enhancing Neuro Imaging Genetics Through Meta Analysis (ENIGMA) Consortium. *Biological Psychiatry* **84**, 644–654 (2018).
76. Harnett, M. T., Makara, J. K., Spruston, N., Kath, W. L. & Magee, J. C. Synaptic amplification by dendritic spines enhances input cooperativity. *Nature* **491**, 599–602 (2012).
77. Hansen, J. Y. *et al.* Correspondence between gene expression and neurotransmitter receptor and transporter density in the human brain. *NeuroImage* **264**, 119671 (2022).
78. Whitfield-Gabrieli, S. & Nieto-Castanon, A. Conn: A Functional Connectivity Toolbox for Correlated and Anticorrelated Brain Networks. *Brain Connectivity* **2**, 125–141 (2012).
79. Mucha, P. J., Richardson, T., Macon, K., Porter, M. A. & Onnela, J. P. Community structure in time-dependent, multiscale, and multiplex networks. *Science* (2010) doi:10.1126/science.1184819.
80. Rubinov, M. & Sporns, O. Complex network measures of brain connectivity: Uses and interpretations. *NeuroImage* **52**, 1059–1069 (2010).
81. Bassett, D. S. *et al.* Robust detection of dynamic community structure in networks. *Chaos* (2013) doi:10.1063/1.4790830.

82. Yeh, F. C., Verstynen, T. D., Wang, Y., Fernández-Miranda, J. C. & Tseng, W. Y. I. Deterministic diffusion fiber tracking improved by quantitative anisotropy. *PLoS ONE* **8**, 1–16 (2013).
83. Naze, S., Proix, T., Atasoy, S. & Kozloski, J. R. Robustness of connectome harmonics to local gray matter and long-range white matter connectivity changes. *NeuroImage* **224**, 117364 (2021).